Study on the Attack of Molten Silicates on Plasma-Sprayed Thermal Barrier Coatings

**Roberto Fernando Martins¹* ⬤, Karl Friehe¹, Cecília Chaves Guedes e Silva²,
Dolores Ribeiro Ricci Lazar², Antônio Augusto Couto¹,², Carlos Roberto Camello Lima¹**

¹School of Engineering, Mackenzie Presbyterian University, São Paulo, Brazil
²Nuclear and Energy Research Institute, São Paulo, Brazil
Email: *roberto.engmec@gmail.com

Abstract

Thermal barrier coating (TBC) revolutionized the industry by allowing higher operating temperatures for equipment, such as gas turbines in the aeronautical industry. However, at high temperatures, the TBC is exposed to the attack of molten silicates, known as CMAS (Calcium-Magnesium-Alumino-Silicate), which are particles from the environment that infiltrate the TBC, causing delamination. In this study, samples coated with TBC by thermal spray and covered with CMAS were evaluated at temperatures of 1200°C and 1250°C. For each temperature, exposure times of 1 h and 5 h were used. Samples with longer exposure time had a considerable volume increase. The main contribution of this work was to demonstrate the non-wettability of the CMAS, even in the 5-h heat treatments, which prevented its infiltration in the deeper regions. The conditions to guarantee the formation of the silicate and its consequent wettability are also discussed.

Keywords

Thermal Barrier Coatings, Molten Silicates, Thermal Spray

1. Introduction

Thermal barrier coating (TBC) is increasingly applied to metallic components that operate at thermally high temperatures, which leads to oxidation and corrosion of these components. The structure of a TBC system consists of two layers: the ceramic top coat and the metallic bond coat, which lies between the metal substrate and the top coat [1].

The ceramic outer layer usually consists of zirconia (ZrO_2) stabilized with 6 to 8% by weight of yttria (Y_2O_3). The top coat is often called YSZ (Yttria Stabilized

Zirconia) or PSZ (Partially Stabilized Zirconia). Its thickness ranges from 130 to 380 μm [1] [2]. This material has low conductivity, high thermal shock tolerance, and a high melting point compared to other oxides. Its main function in TBC is the thermal insulation of the metal substrate [1] [2] [3] [4] [5]. The thickness of the bond coat varies between 60 and 160 μm. It usually consists of an MCrAlY alloy ("M" signifying Co, Fe, and Ni, or a combination of these). The choice of this alloy is largely due to its high resistance to oxidation and corrosion when operating at elevated temperatures. Thus, the two main functions of the bond coat are 1) to protect the substrate against oxidation and corrosion at high temperatures and 2) to promote adhesion between the substrate and the ceramic top layer [1] [2] [3] [4] [6].

The efficiency provided by a TBC system is unquestionable. The superalloys in turbine components generally operate above 1370˚C, but with a melting point of around 1300˚C. The airfoils are manufactured hollow to avoid structural failure by melting, oxidation, thermal fatigue, or other mechanisms. In addition, a stream of compressed air is injected to cool the component [7] [8]. A TBC system can reduce the surface temperature of the component by approximately 170˚C. This thermal insulation can increase gas turbine efficiency, reduce maintenance requirements, reduce fuel consumption, and increase by 3 to 4 times the life of the coated component [2] [3] [7] [8] [9].

The two main techniques currently used to fabricate YSZ are Air Plasma Spray (APS) and Electron Beam-Physical Vapor Deposition (EB-PVD) [3] [10] [11] [12] [13]. Rotating components such as turbine blades, which are always subject to thermal stress cycles, are preferably manufactured using EB-PVD, which can increase the tolerance of these elements [11] [12]. Rotation of the component during the deposition process creates a columnar structure with intercolumnar gaps [6]. In contrast, stationary objects, such as combustion cylinders and turbines, are manufactured by APS [3] [12]. The microstructure produced is a thin lamellar layer (typical of thermal spray), with pores, microcracks, oxides, and solid particles between the lamellae of the coating [1] [12] [14]. In addition, the APS technique is used more than EB-PVD because it is easier to apply and less expensive [3].

Spallation, the main failure mode of a TBC system, occurs due to the emergence of residual stresses in the system, caused by the oxidation of the bond coat during operation at elevated temperatures and by the difference in the thermal expansion coefficients of the bond coat and the top coat [1] [4] [15]. Buckling followed by spallation can occur in the system as the coating is subjected to compressive residual stresses due to the difference in thermal expansion coefficients between the substrate and the coating [6]. In recent years, the scientific community has turned its attention to the attack promoted by molten silicates, which are usually referred as CMAS because of their main components: Calcium-Magnesium-Alumino-Silicate. This attack occurs because the YSZ is an extremely porous layer. As the equipment operates at high temperatures, deposits from the environment, including dust, sand, volcanic ash, and runway de-

bris, melt and penetrate the porous structure of the TBC [4] [16] [17] [18]. Inside the TBC, the CMAS promotes a thermochemical attack, as the YSZ dissolves in the presence of the CMAS and reprecipitates with different compositions and morphology [16]. The CMAS also performs a thermomechanical attack. This occurs because, during turbine cooling, the CMAS solidifies inside the YSZ, increasing its stiffness and promoting the spallation of the system [18] [19] [20].

This study aims to evaluate typical TBC (YSZ) samples subjected to CMAS attack at different operating temperatures and for different exposure times at these temperatures, correlating with the wettability of the molten silicates in the ceramic structure of the TBC.

2. Materials and Methods

2.1. Preparation of the CMAS

A specific composition of the CMAS was prepared based on the literature [10] [16] [17] [21]. The following chemical reagents were used: CaO (DINÂMICA QUÍMICA, 95% purity), MgO (CAAL, 95% purity), Al_2O_3 (NEON, 95% purity), and SiO_2 (ADICEL, 94% purity). The oxides were placed in a Petri dish and mixed with a spatula until uniform coloration was achieved. Table 1 details the percentage by weight of each component in the manufactured CMAS. It is important to mention that the constitution of the CMAS may vary depending on the place of origin [18].

2.2. Obtaining the Samples

The original TBC sample was fabricated on a carbon steel substrate. The APS technique in an argon-hydrogen atmosphere, using an F4 plasma torch (Oerlikon Metco, F4MB), configured with a 6 mm nozzle and 1.8 mm injector, was employed to deposit both the bond coat and the top coat. The bond coat was made of NiCrAl alloy and the ceramic layer was ZrO_2-7%Y_2O_3 (Oerlikon Metco). A PACE cutter, model PICO 155 Precision Saw, was used to cut the original sample into six smaller specimens. Each of these specimens was approximately $17 \times 17 \times 4$ (Dimensions in mm). Of these six samples obtained, one was left as a spare and the other five were used for the study and were numbered 0, 1, 2, 3, and 4.

Table 1. Constituents of the produced CMAS.

Oxide	Content (wt%)
SiO_2	48.4
CaO	33.2
Al_2O_3	12.0
MgO	6.4
CMAS (Total)	100.0

2.3. Isothermal Treatments

For the isothermal treatment cycles, a Lindberg/Blue M Tube Furnace was used. On each isothermally treated sample, approximately 10 mg/cm^2 of CMAS was manually deposited on its surface before being placed in the furnace. To facilitate reading and understanding of the work, the samples were renamed according to the isothermal treatment applied. Sample 0 did not receive isothermal treatment. The other samples (1 to 4) were initially heated with a linear ramp of 10˚C/min from room temperature (25˚C) to a temperature of 1000˚C. Subsequently, there was a secondary heating process that used a linear ramp of 5˚C/min. Finally, the samples were slowly cooled to room temperature. Table 2 shows the secondary heating process, the length of stay and the designation adopted for the samples.

2.4. Energy Dispersive X-Ray Spectroscopy (EDS)

After isothermal treatment, the samples in Table 2 were cut, embedded in Bakelite, sanded, and polished to obtain a flat, mirror-like surface and evaluate their respective cross sections. To visualize the chemical components on the surfaces of the polished samples, the energy dispersive x-ray spectroscopy (EDS) technique was used. This technique was performed using a JEOL scanning electron microscope (SEM), model JSM-6510.

3. Results and Discussions

3.1. Wettability

Photographs taken with conventional equipment show the top view of the TBC samples to analyze the wettability of the CMAS (Figure 1). Figure 1(a) presents sample 0, untreated. Figure 1(b) illustrates sample 1-1200-1 with the deposition of 10 mg/cm^2 of CMAS before the isothermal treatment. Images of samples 1-1200-1, 2-1200-5, 3-1250-1, and 4-1250-5 after the isothermal treatments are in Figures 1 (c)-(f), respectively.

After the isothermal treatments, the particle size of the deposited CMAS was modified. The material maintained a light coloration, but the grains joined together, visually increasing the grain size of the CMAS. Cracks visible to the naked eye appeared in samples 2-1200-5 and 4-1250-5 (Figure 1(d) and Figure 1(f)). These samples were subjected to a longer exposure time (5 h) at their

Table 2. Secondary heating process, length of stay and adopted designation.

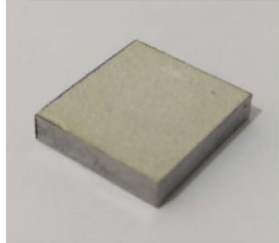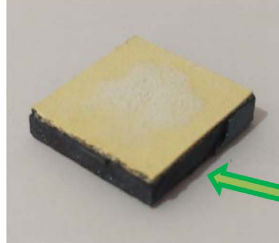| Sample	Secondary Heating Process	Length of Stay	Adopted Designation
0	-	-	0
1	1000˚C - 1200˚C	1 hour	1-1200-1
2	1000˚C - 1200˚C	5 hours	2-1200-5
3	1000˚C - 1250˚C	1 hour	3-1250-1
4	1000˚C - 1250˚C	5 hours	4-1250-5
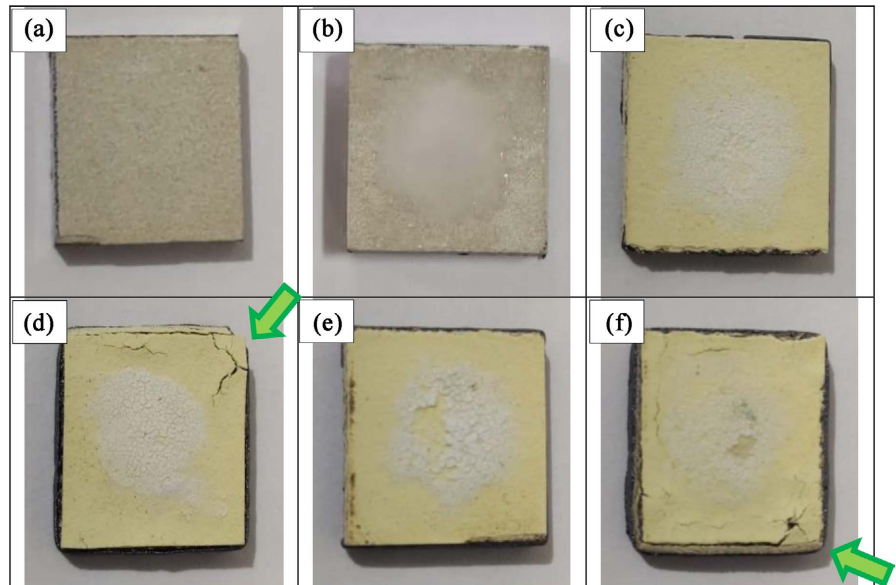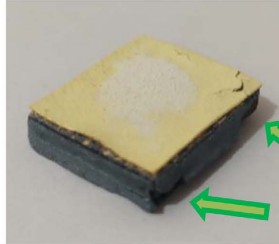
Figure 1. Wettability analysis: (a) Sample 0; (b) Sample 1-1200-1 before IT; (c) Sample 1-1200-1 after IT; (d) Sample 2-1200-5 after IT; (e) Sample 3-1250-1 after IT; (f) Sample 4-1250-5 after IT (IT—Isothermal Treatment).

respective isothermal treatment temperatures, therefore, the exposure time was more detrimental to the coating than the applied temperature. Wettability was not observed under the tested conditions. The area occupied by the deposited CMAS remained approximately the same before and after isothermal treatments (Figures 1(b)-(f)). Thus, it can be assumed that no silicate was formed or that only a small amount was formed. Two different ways to produce CMAS are found in the literature. In the former, the components are mixed in appropriate proportions and applied to the surface of the samples [16] [22] [23] [24] [25]. In the second, after mixing the components, a heat treatment is done before applying the material to the samples. This heat treatment aims to ensure the formation of silicate [18] [26] [27] [28] [29]. In this study, the first methodology was adopted because it is closer to the operation of gas turbines. It is important to mention that some of the applied material may have become silicate and penetrated the YSZ. Thus, a cross-sectional analysis of the samples is necessary to determine whether or not the molten silicates infiltrated into the TBC.

3.2. Variation in Volume

Figure 2 shows the conventional equipment images (frontal and isometric) of samples 1-1200-1, 2-1200-5, 3-1250-1, and 4-1250-5 after their respective isothermal treatments. Images of sample 0 (no treatment) are also shown for comparison.

The height of the samples in Figure 2 was measured with a caliper. Samples 2-1200-5 and 4-1250-5 had a greater increase in height (around 20%) and consequently in volume. A comparison of samples 2-1200-5 and 3-1250-1 demonstrated that exposure time had a greater influence than the temperature on

Figure 2. Variation in the sample volume: Frontral View and Isometric View [dimensions in mm].

volume increase. Buckling can be observed in sample 2-1200-5. Severe corrosion was also observed on the steel substrates (indicated by arrows in **Figure 2**). This is because the sides of the obtained samples were exposed to the environment after cutting the original sample, causing hot oxidation on the steel substrates during the isothermal treatments.

CMAS can increase the volume of the TBC by penetrating the YSZ. In the presence of molten silicates, the YSZ grains dissolve easily. As a result, a phase transformation occurs in YSZ, which originally had a tetragonal structure that precipitated into a monoclinic structure. This phase transformation is accompa-

nied by an increase in volume. Furthermore, once inside the coating, the CMAS can separate the crystals from the structure, implying a further increase in volume [21] [22] [30]. However, to infiltrate the TBC structure through pores and microcracking, CMAS must melt [31] to form silicate. However, because no wettability was observed, silicate formation probably did not occur, and thus penetration did not occur, or if it did, it was a small amount of material. Therefore, the oxidation corrosion of the substrates is the main factor related to the observed volume increase, since iron oxidation involves the absorption of oxygen from the atmosphere, which implies an increase in the mass of the oxidized substrate.

In addition to the oxidation of the substrate, it should also be mentioned the appearance of some cracks in the samples after the isothermal treatments. As previously mentioned, the original structure of a TBC system consists of two layers (bond coat and top coat) deposited on the substrate. In Figure 3 this structure can be seen by the scanning electron microscope (SEM) image.

The samples tested for a 5-hour interval showed the appearance of cracks in their structures, which is also one of the reasons for the observed increase in volume (Figure 4).

3.3. Energy Dispersive X-Ray Spectroscopy (EDS)

The cross-section of the samples was examined using EDS to observe the permeability of the molten silicates inside the ceramic layer of the TBC. For each analysis elements with a lower percentage of weight and/or irrelevant for this study were disregarded. Figure 5 illustrates the overview of sample 0, which allows the constituent elements of TBC to be identified.
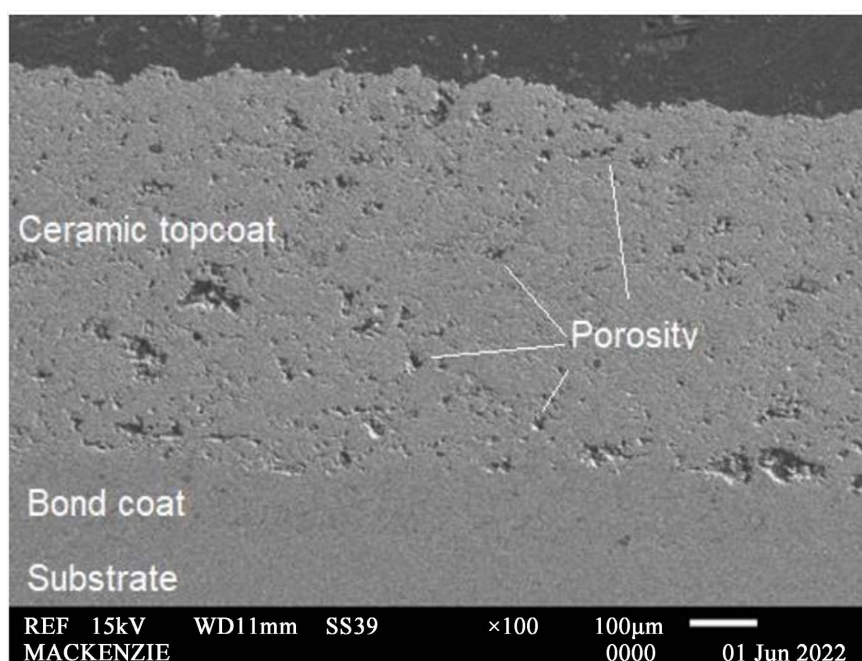
Figure 3. SEM of cross section of the as sprayed TBC.
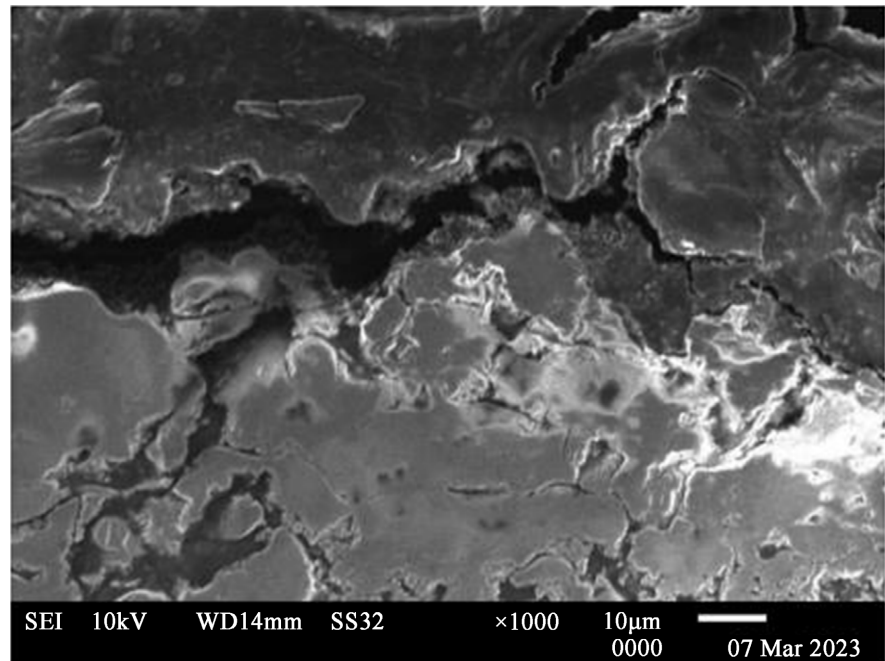
Figure 4. SEM. Cracks presents in the sample 4-1250-5 after exposition to 5 hours at 1250˚C.

Figure 5. EDS overview of Sample 0.

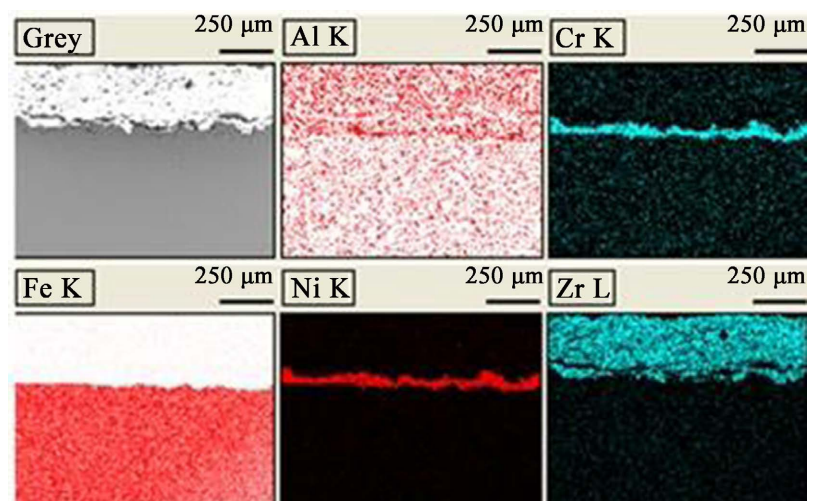Three distinct regions can be seen in **Figure 5**. At the bottom, the intense amount of Fe demonstrates that this is the steel substrate. In the upper region, the Zr element appears more intensely, indicating the top coat region (YSZ). The bond coat can be identified by the presence of the elements Ni, Cr, and Al (although Al is distributed throughout the region, a greater concentration is noticeable in the bond coat region). Therefore, a NiCrAl-type alloy is evident in the bond coat.

Figure 6 illustrates an EDS image focused on the ceramic coating of sample 0. In this image, the presence of Y is visible, due to the higher magnification. Oxygen also appears throughout the region. This element is present in zirconia

(ZrO_2) and yttria (Y_2O_3). However, the sample surface could also have oxidation, as the sample had contact with the atmosphere after polishing and before being inserted into the sample holder of the SEM.

The ceramic coating of sample 1-1200-1 presented in Figure 7 illustrates the ceramic layer (Zr), bond coat (Ni and Cr), and part of the substrate (Fe). Therefore, it was not possible to identify regions with infiltration of molten silicates in sample 1-1200-1. The short exposure time may not have been sufficient to melt CMAS and penetrate the coating structure; therefore, the deposited material remained on the YSZ surface [31].

An EDS image of sample 2-1200-5 is in Figure 8. A linear concentration of Ca is recorded in the upper part of the plate, indicating that CMAS is present on the surface of the ceramic layer. However, the upper right region shows a higher concentration of both Ca and Mg. In the same region, no presence of Zr and Y
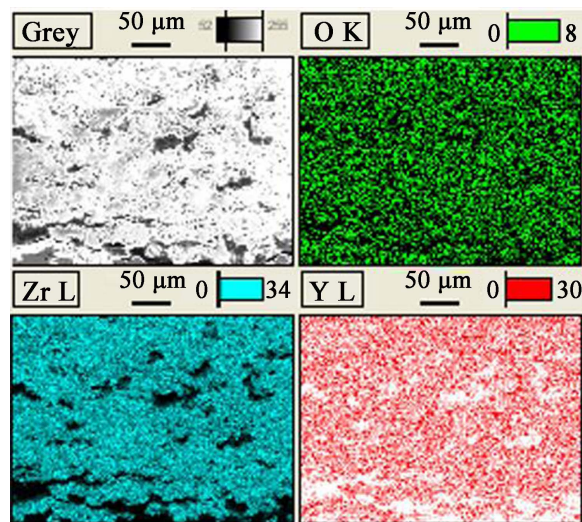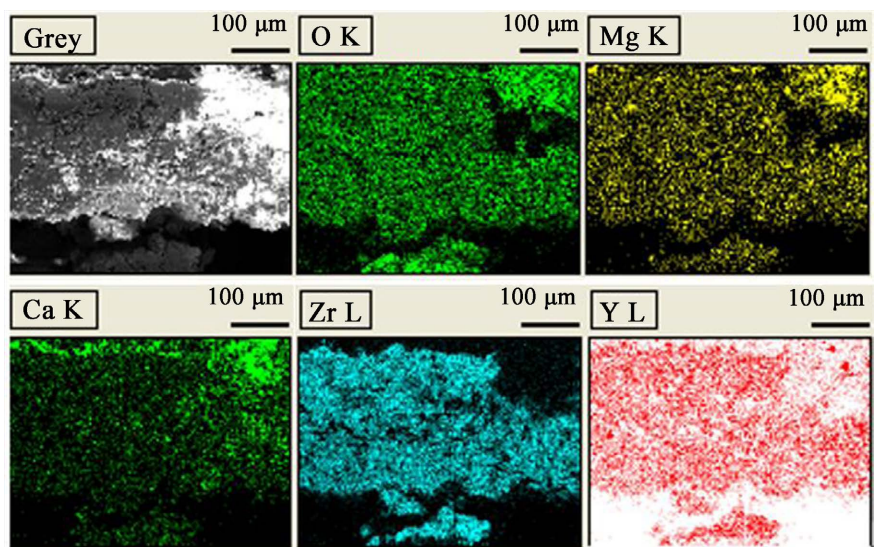

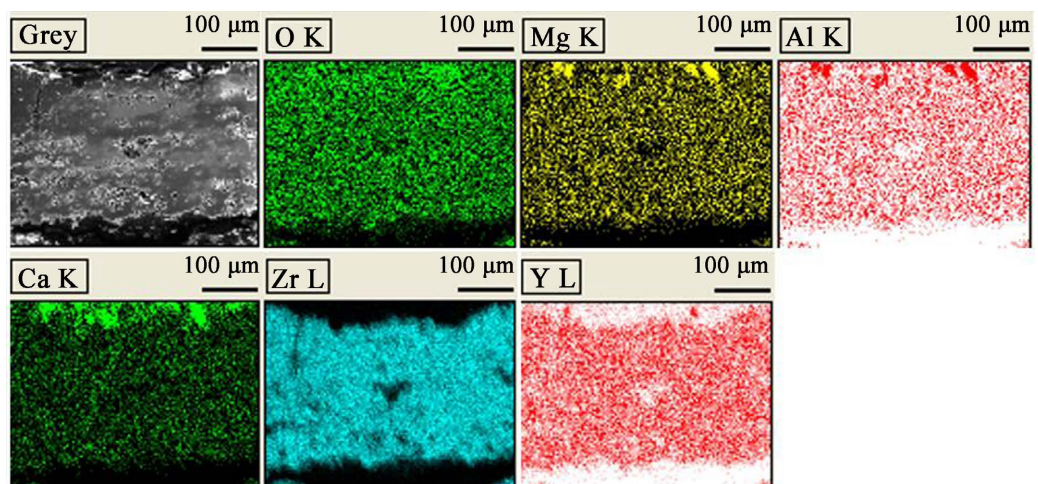**Figure 6.** Sample 0. Image obtained by EDS of the ceramic coating.
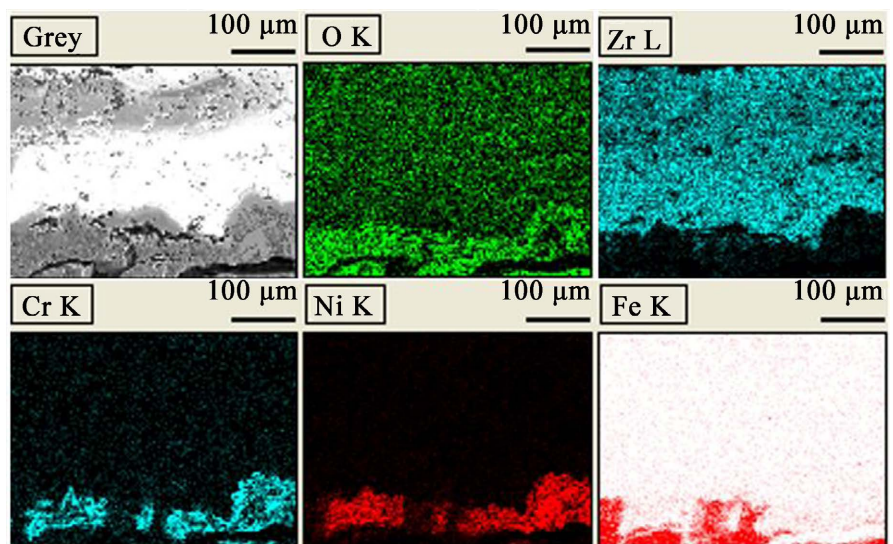
Figure 7. Sample 1-1200-1. Image obtained by EDS of the ceramic coating.

appears in lower concentrations, which indicates the accumulation of CMAS in the region of YSZ discontinuity. However, this discontinuity may have been caused by the CMAS itself through a chemical corrosion process [16] [20]. The small amount of Y in this region reinforces this hypothesis since a discontinuity due to mechanical friction would imply the complete absence of both Zr and Y. At an intermediate depth, a greater concentration of Ca is noted on the right than in the left region, evidencing that the high concentration in the upper region allowed greater infiltration, including in regions with Zr and Y. This is because the amount of CMAS has a large effect on the severity of the corrosion. Factors that influence the penetration of CMAS inside the TBC are temperature, time, the surface roughness of the YSZ, and the number of molten silicates. The higher the amount of CMAS in the region, the greater the observed degradation effects and the greater the penetration depth achieved [32] [33].

The ceramic layer of sample 3-1250-1 is illustrated in **Figure 9**.

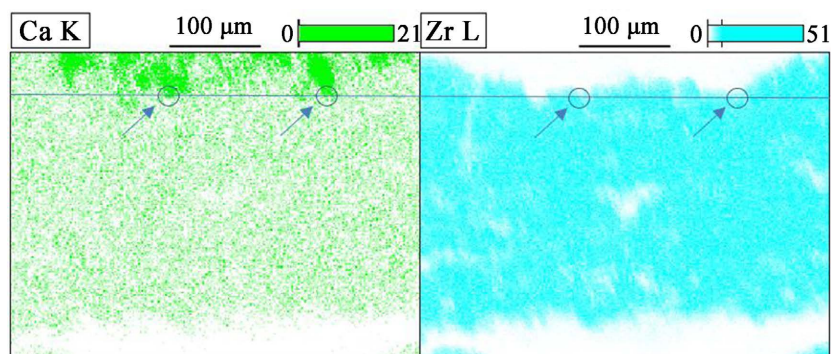**Figure 8.** Sample 1-1200-5. Image obtained by EDS of the ceramic coating.

Figure 9. Sample 3-1250-1. Image obtained by EDS of the ceramic coating.

The constituent elements of yttria-stabilized zirconia (Zr, Y, and O) are easily identifiable in Figure 9. The elements of interest—Ca, Mg, and Al (CMAS constituents)—appear at higher concentrations above the ceramic coating.

However, a comparison between Zr and Ca indicates an apparent overlap between these elements at the CMAS interface with the YSZ. This means that a small amount of CMAS infiltration occurred in the surface region of the YSZ. The infiltration process of CMAS has the following sequence: 1) Through wettability, the molten CMAS spreads along the surface of the TBC. During this propagation process on the surface, the dynamic contact angle decreases dramatically over time. 2) Upon reaching a steady state of spreading, the infiltration process begins, which is believed to start through the surface defects, such as microcracks formed during the coating deposition process. 3) Once inside the ceramic layer, the molten CMAS propagates through microstructure defects, mainly wide-open cracks [32]. Figure 10 shows the beginning of penetration (*i.e.*, stage 2).

Figure 11 shows the EDS image for sample 4-1250-5. The constituent elements of the YSZ (Zr, Y, and O) appear to be well distributed in the analyzed region. However, no relevant quantities of the participating CMAS elements (Ca, Mg, Al, and Si) were found, indicating the absence of silicate in the analyzed region. The exposure time influences the penetration depth of the CMAS into the ceramic layer, which may reach the bond coat or even the substrate [22] [31] [34] [35]. However, the literature indicates that 5 h at 1250°C is sufficient for complete penetration of CMAS into the YSZ [21]. This also evidences that silicate formation did not occur or only a small amount was formed.

To better observe the penetration, one of the possibilities is to ensure the formation of the silicate, *i.e.*, as mentioned earlier, some authors performed a heat treatment on the mixture of the CMAS constituents before depositing it onto TBC samples. This heat treatment requires a high temperature and exposure time to ensure silicate formation, such as 1400°C for the time interval of 30 min [18] or 1 h [21]. Another possibility is to focus a higher magnification on the surface of the ceramic layer since CMAS accumulates on the surface of the top coat when there is no penetration [31]. An investigation in the pore and microcrack regions, which are pathways for CMAS [36], could be evidence of the

Figure 10. Sample 3-1250-1. Comparison between Ca and Zr elements.
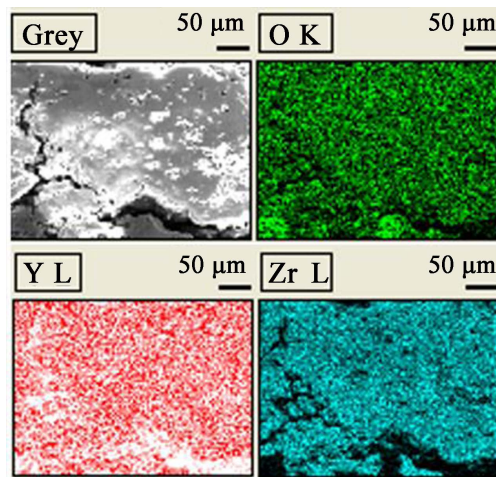
Figure 11. Sample 4-1250-5. Image obtained by EDS of the ceramic coating.
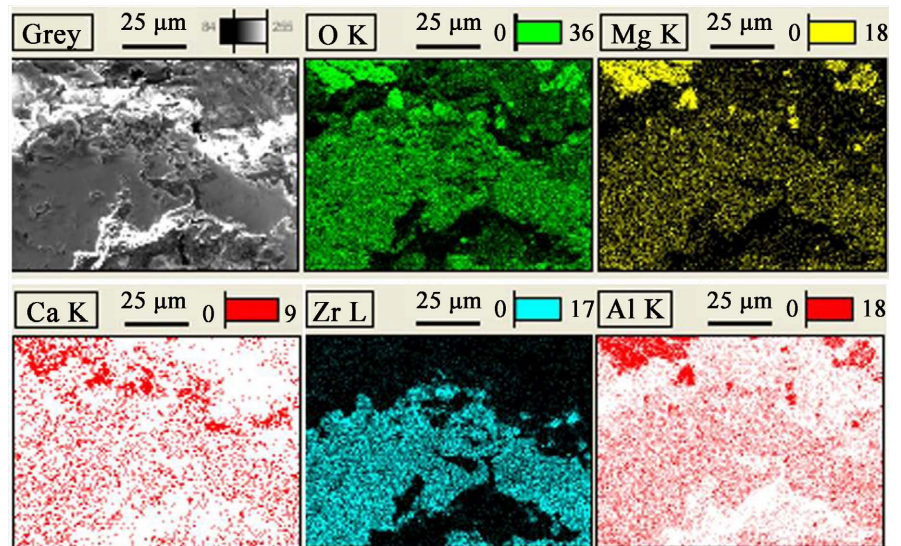
Figure 12. Sample 4-1250-5. Image obtained by EDS focusing on the top surface of the ceramic coating.

beginning of penetration.

Figure 12 shows the EDS image that was focus on the surface layer of sample 4-1250-5. In the left upper region is possible to observe a great amount of Ca, Mg and Al (constituents of CMAS) indicating the presence of these elements, but these tree elements (together) are above on the surface of YSZ when compared to Zr. On the other side, the comparison between only Ca and Zr allow to observe that in some regions a superficial penetration has occurred how is showed in Figure 13. This penetration was very superficiality, similar to that which occurred in sample 3-1250-1 (Figure 10).

4. Conclusions

None of the test conditions showed CMAS's wettability on the surface of the TBCs, indicating the need for heat treatments with longer exposure time or
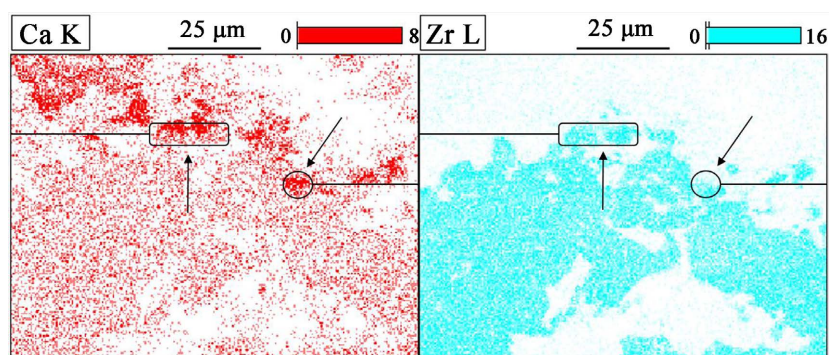
Figure 13. Sample 4-1250-5. Comparison between Ca and Zr elements.

higher service temperatures for complete silicate formation. The methodology of performing a heat treatment of the CMAS before application to the samples is also a viable possibility.

The steel substrates suffered from hot corrosion because the sides of the samples were exposed to the furnace atmosphere during isothermal treatments, allowing oxidation corrosion.

The samples treated isothermally for the 5-h interval (2-1200-5 and 4-1250-5) showed the largest volume increase. This increase occurred due to emergence of some cracks and mainly due to the hot corrosion of the steel substrate.

The CMAS permeability within the YSZ was not observed in sample 1-1200-1. A small amount of infiltration into the surface region of the ceramic layer was observed for samples 3-1250-1 and 4-1250-5. A longer exposure time would facilitate the infiltration of the molten silicates into the deeper regions of the coating.

On the other side, sample 2-1200-5 displayed the penetration of molten silicates into the interior of the TBC. The CMAS penetration reached greater depths in the region with the highest accumulation of CMAS on the surface of the ceramic layer.

For future research, a study focused on determining the necessary conditions for the formation of silicate with the composition used here is suggested. For this, the CMAS produced must be submitted to different isothermal treatments (varying the temperature and time of each one of them), and analyzing the formation or not of the silicate according to the isothermal treatment applied. This study should precisely target test conditions for a new penetration assessment of CMAS in TBC.

Acknowledgements

Conflicts of Interest

The authors declare no conflicts of interest regarding the publication of this paper.

References

[1] Lima, C.R.C. and Trevisan, R.E. (2007) Aspersão Térmica: Fundamentos e Aplicações. 2nd Edition, Artliber Ltd., São Paulo.

[2] Xu, H., Gong, S. and Deng, L. (1998) Preparation of Thermal Barrier Coatings for Gas Turbine Blades by EB-PVD. *Thin Solid Films*, **334**, 98-102. https://doi.org/10.1016/S0040-6090(98)01124-9

[3] Oliveira, J.P. and Duarte, J.F. (2013) Revestimentos Cerâmicos Utilizados como Barreira Térmica. *Cerâmica*, **59**, 186-191. https://doi.org/10.1590/S0366-69132013000100023

[4] Lima, C.R.C. (2014) Revestimentos para Barreira Térmica: Evolução e Perspectivas. *Soldagem & Inspeção*, **19**, 353-363. https://doi.org/10.1590/0104-9224/SI1904.11

[5] Hardwicke, C.U. and Lau, Y.-C. (2013) Advances in Thermal Spray Coatings for Gas Turbines and Energy Generation: A Review. *Journal of Thermal Spray Technology*, **22**, 564-576. https://doi.org/10.1007/s11666-013-9904-0

[6] Clarke, D.R. and Levi, C.G. (2003) Materials Design for the Next Generation Thermal Barrier Coatings. *Annual Review of Materials Research*, **33**, 383-417. https://doi.org/10.1146/annurev.matsci.33.011403.113718

[7] Meier, S.M. and Gupta, D.K. (1992) The Evolution of Thermal Barrier Coatings in Gas Turbine Engine Applications. *Proceedings of the ASME* 1992 *International Gas Turbine and Aeroengine Congress and Exposition*, *Cologne*, 1-4 June 1992. https://doi.org/10.1115/92-GT-203

[8] Padture, N.P., Gell, M. and Jordan, E.H. (2002) Thermal Barrier Coatings for Gas-Turbine Engine Applications. *Science*, **296**, 280-284. https://doi.org/10.1126/science.1068609

[9] Moskal, G. (2009) Thermal Barrier Coatings: Characteristics of Microstructure and Properties, Generation and Directions of Development of Bond. *Journal of Achievements in Materials and Manufacturing Engineering*, **37**, 323-331. http://jamme.acmsse.h2.pl/papers_vol37_2/37216.pdf

[10] Mohan, P., Patterson, T., Yao, B. and Sohn, Y. (2010) Degradation of Thermal Barrier Coatings by Fuel Impurities and CMAS: Thermochemical Interactions and Mitigation Approaches. *Journal of Thermal Spray Technology*, **19**, 156-167. https://doi.org/10.1007/s11666-009-9424-0

[11] Sampath, S., Schulz, U., Jarligo, M.O. and Kuroda, S. (2012) Processing Science of Advanced Thermal-Barrier Systems. *Materials Research Society Bulletin*, **37**, 903-910. https://doi.org/10.1557/mrs.2012.233

[12] Song, W. and Guo, H. (2022) CMAS Dilema in Jet Engines: Beginning or Ending? *Materials Lab*, **1**, Article ID: 220042. https://doi.org/10.54227/mlab.20220042

[13] Lima, R.S., Zhu, D. and Li, L. (2013) Thermal and Environmental Barrier Coatings (TBCs/EBCs) for Turbine Engines. In: Tucker Jr., R.C., Ed., *Thermal Spray Technology*, *ASM Handbook*, Volume 5A, ASM International, Ohio, 70-279. https://doi.org/10.31399/asm.hb.v05a.a0005733

[14] Bhatia, A. (1999) Thermal Spraying Technology and Applications. U.S. Army Corps of Engineers, Washington DC.

[15] Kyaw, S., Jones, A. and Hyde, T. (2013) Predicting Failure within TBC System: Finite Element Simulation of Stress within TBC System as Affected by Sintering of APS TBC, Geometry of Substrate and Creep of TGO. *Engineering Failure Analysis*, **27**, 150-164. https://doi.org/10.1016/j.engfailanal.2012.07.005

[16] Krämer, S., Yang, J., Levi, C.G. and Johnson, C.A. (2006) Thermochemical Interaction of Thermal Barrier Coatings with Molten CaO-MgO-Al_2O_3-SiO_2 (CMAS) Deposits. *Journal of the American Ceramic Society*, **89**, 3167-3175.
https://doi.org/10.1111/j.1551-2916.2006.01209.x

[17] Pujol, G., Ansart, F., Bonino, J.-P., Mailé, A. and Hamadi, S. (2013) Step-by-Step Investigation of Degradation Mechanisms Induced by CMAS Attack on YSZ Materials for TBC Applications. *Surface & Coatings Technology*, **237**, 71-78.
https://doi.org/10.1016/j.surfcoat.2013.08.055

[18] Rai, A.K., Bhattacharya, R.S., Wolfe, D.E. and Eden, T.J. (2010) CMAS-Resistant Thermal Barrier Coatings (TBC). *International Journal of Applied Ceramic Technology*, **7**, 662-674. https://doi.org/10.1111/j.1744-7402.2009.02373.x

[19] Mercer, C., Faulhaber, S., Evans, A.G. and Darolia, R. (2005) A Delamination Mechanism for Thermal Barrier Coatings Subject to Calcium-Magnesium-Alumino-Silicate (CMAS) Infiltration. *Acta Materialia*, **53**, 1029-1039.
https://doi.org/10.1016/j.actamat.2004.11.028

[20] Morelli, S., Bursich, S., Testa, V., Bolelli, G., Miccichè, A. and Lusvarghi, L. (2022) CMAS Corrosion and Thermal Cycling Fatigue Resistance of Alternative Thermal Barrier Coating Materials and Architectures: A Comparative Evaluation. *Surface & Coatings Technology*, **439**, Article ID: 128433.
https://doi.org/10.1016/j.surfcoat.2022.128433

[21] Han, J., Zou, Y., Wu, D., Chen, J. and Zhang, Y. (2022) Improving CMAS-Corrosion Resistance of YSZ-Based Thermal Barrier Coatings with Al_2O_3 Addition. *Surface & Coatings Technology*, **446**, Article ID: 128799.
https://doi.org/10.1016/j.surfcoat.2022.128799

[22] Wu, J., Guo, H.-B., Gao, Y.-Z. and Gong, S.-K. (2011) Microstructure and Thermo-Physical Properties of Yttria Stabilized Zirconia Coatings with CMAS Deposits. *Journal of the European Ceramic Society*, **31**, 1881-1888.
https://doi.org/10.1016/j.jeurceramsoc.2011.04.006

[23] Li, M., Cheng, Y., Guo, L., Zhang, Y., Zhang, C., He, S., Sun, W. and Ye, F. (2017) Preparation of Nanostructured $Gd_2Zr_2O_7$-$LaPO_4$ Thermal Barrier Coatings and their Calcium-Magnesium-Alumina-Silicate (CMAS) Resistance. *Journal of the European Ceramic Society*, **37**, 3425-3434.
https://doi.org/10.1016/j.jeurceramsoc.2017.03.069

[24] Krämer, S., Yang, J. and Levi, C.G. (2008) Infiltration-Inhibiting Reaction of Gadolinium Zirconate Thermal Barrier Coatings with CMAS Melts. *Journal of the American Ceramic Society*, **91**, 576-583.
https://doi.org/10.1111/j.1551-2916.2007.02175.x

[25] Gao, L., Guo, H., Gong, S. and Xu, H. (2014) Plasma-Sprayed $La_2Ce_2O_7$ Thermal Barrier Coatings Against Calcium-Magnesium-Alumina-Silicate Penetration. *Journal of the European Ceramic Society*, **34**, 2553-2561.
https://doi.org/10.1016/j.jeurceramsoc.2014.02.031

[26] Xiao, H., Cheng, Y., Yu, L. and Liu, H. (2006) A Study on the Penetration of CMAS Glass-Ceramics by *in Situ*-Crystallization. *Materials Science and Engineering: A*, **431**, 191-195. https://doi.org/10.1016/j.msea.2006.05.153

[27] Wang, Y., Xu, Z., Wang, W., Zhang, C., Yu, Z., Fang, H. and Yang, T. (2022) Prep-

aration and CMAS Wettability Investigation of CMAS Corrosion Resistant Protective Layer with Micro-Nano Double Scale Structure. *Coatings*, **12**, Article No. 648. https://doi.org/10.3390/coatings12050648

[28] Fang, H., Wang, W., Huang, J. and Ye, D. (2019) Corrosion Resistance and Thermal-Mechanical Properties of Ceramic Pellets to Molten Calcium-Magnesium-Alumina-Silicate (CMAS). *Ceramics International*, **45**, 19710-19719. https://doi.org/10.1016/j.ceramint.2019.06.223

[29] Sun, Y., Xiang, H., Dai, F.-Z., Wang, X., Xing, Y., Zhao, X. and Zhou Y. (2021) Preparation and Properties of CMAS Resistant Bixbyite Structured High-Entropy Oxides RE_2O_3 (RE = Sm, Eu, Er, Lu, Y, and Yb): Promising Environmental Barrier Coating Materials for Al_2O_{3f}/Al_2O_3 Composites. *Journal of Advanced Ceramics*, **10**, 596-613. https://doi.org/10.1007/s40145-021-0461-6

[30] Shan, X., Zou, Z., Gu, L., Yang, L., Guo, F., Zhao, X. and Xiao, P. (2016) Buckling Failure in Air-Plasma Sprayed Thermal Barrier Coatings Induced by Molten Silicate Attack. *Scripta Materialia*, **113**, 71-74. https://doi.org/10.1016/j.scriptamat.2015.09.029

[31] Guo, L., Gao, Y., Cheng, Y., Sun, J., Ye, F. and Wang, L. (2021) Microstructure Design of the Laser Glazed Layer on Thermal Barrier Coatings and Its Effect on the CMAS Corrosion. *Corrosion Science*, **192**, Article ID: 109847. https://doi.org/10.1016/j.corsci.2021.109847

[32] Ma, X., Ruggiero, P. and Wildridge, G. (2022) Evaluation of CMAS Resistance and Failure Behavior for Phase Composite Thermal Barrier Coatings. *Proceedings of the ITSC*2022. *Thermal Spray* 2022: *Proceedings from the International Thermal Spray Conference*, Vienna, 4-6 May 2022, 14-24. https://doi.org/10.31399/asm.cp.itsc2022p0014

[33] Yin, B., Liu, Z., Yang, L., Wu, R. and Zhou, Y. (2019) Factors Influencing the Penetration Depth of Molten Volcanic Ash in Thermal Barrier Coatings: Theoretical Calculation and Experimental Testing. *Results in Physics*, **13**, Article ID: 102169. https://doi.org/10.1016/j.rinp.2019.102169

[34] Ozgurluk, Y., Doleker, K.M., Ahlatci, H. and Karaoglanli, A.C. (2021) Investigation of Calcium-Magnesium-Alumino-Silicate (CMAS) Resistance and Hot Corrosion Behavior of YSZ and $La_2Zr_2O_7$/YSZ Thermal Barrier Coatings (TBCs) Produced with CGDS Method. *Surface & Coatings Technology*, **411**, Article ID: 126969. https://doi.org/10.1016/j.surfcoat.2021.126969

[35] Nieto, A., Agrawal, R., Bravo, L., Hofmeister-Mock, C., Pepi, M. and Ghoshal, A. (2020) Calcia-Magnesia-Alumina-Silicate (CMAS) Attack Mechanisms and Roadmap towards Sandphobic Thermal and Environmental Barrier Coatings. *International Materials Reviews*, **66**, 451-492. https://doi.org/10.1080/09506608.2020.1824414

[36] Shan, X., Luo, L., Chen, W., Zou, Z., Guo, F., He, L., Zhang, A., Zhao, X. and Xiao, P. (2018) Pore Filling Behavior of YSZ under CMAS Attack: Implications for Designing Corrosion-Resistant Thermal Barrier Coatings. *Journal of the American Ceramic Society*, **101**, 5756-5770. https://doi.org/10.1111/jace.15790